CHARACTERISTICS OF EXPANSIVE CLAY ROUGHNESS OF PAVEMENTS

Robert L. Lytton, Ronald L. Boggess, and J. W. Spotts, Texas A&M University

The patterns of pavement roughness caused by expansive clay appear to be predictable from the mineralogical and pedologic properties of the clay deposit. Surveying measurements made in two gilgai fields with similar mineralogy reveal a high degree of statistical similarity in wavelengths and amplitudes of the surface waves. Field measurements of water content, suction, density, and horizontal and vertical displacements of the soil with depth throughout one weather cycle beneath the mounds and the depressions have revealed the mechanism of differential heaving of these expansive clay deposits. Pavement roughness was measured on pavements adjacent to the gilgai fields and on other pavement sections by the GM profilometer. Digital magnetic tapes of the profilometer data are analyzed by a series of digital filters especially designed for expansive clay wavelengths. Statistical data on the wavelengths and amplitudes of these typical expansive clay roughness patterns are determined and compared with those measured in the gilgai fields where these patterns have not been tampered with. The riding characteristics of these pavements as measured by the Mays meter are analyzed with a computerized model of a vehicle that is programmed to accept GM profilometer data. Dynamic load factors for the actual pavements are determined. Equations are presented that give Mays meter readings and dynamic load factors for any combination of expansive clay wavelengths and amplitudes. The effect of the dynamic load on reducing the service life of the pavement is discussed, and methods of predicting level-up and overlay quantities from the characteristics of expansive clay roughness are given.

•THE major effects of expansive clay roughness on pavements are a loss of riding comfort and road-holding ability, a reduction in pavement service life, and the costliness of the rehabilitation that is required. In those areas where expansive clays exist, they take up a substantial portion of the annual maintenance budget. Identification of expansive clays in the field is simple compared with determination of the most economic strategy to follow in preserving acceptable riding quality. This complexity is based on the fact that there have been no consistent measures of roughness that can be used to estimate the quantities of reworking, releveling, and overlaying that will be required to restore riding quality. This paper presents a hypothesis about expansive clay roughness that is based on the natural morphology of the soil surface and the cracking patterns that expansive clays tend to form when they are exposed to wetting and drying influences. A study of natural soil shapes reveals pavement roughness patterns that may be expected to develop over a period of time when a pavement has been built on expansive clay. Roughness is based on crack spacing, which, in turn, is based on the mineralogy of the soil. The natural roughness patterns are called gilgai, and these are compared with the roughness patterns measured on adjacent pavements. Amplitude versus wavelength and wavelength distributions for both pavement and natural soils are compared for two different geological formations within Texas. Although they are separated by 50 miles (80.5 km) in distance and hundreds of thousands of years in deposition history, their mineralogy is almost the same, and, consequently, it is expected that their roughness patterns are statistically similar. From the pavement roughness data, a relation among serviceability, amplitude, and wavelength is derived and is used to

analyze riding quality with a computer-simulated Mays meter response as the indicator of riding quality. The expansive clay roughness of the pavement will also cause dynamic loads to be applied, thus conceivably shortening the pavement service life. The size and importance of dynamic loads caused by expansive clay roughness on service life and methods of predicting future rehabilitation requirements are discussed. The potential usefulness of this kind of characterization of expansive clay roughness is in permitting the designer to calculate the costs of future rehabilitation and compare the present value of those costs with the costs of preconstruction treatments that may be used to reduce the development of future roughness.

GILGAI—NATURAL EXPANSIVE CLAY ROUGHNESS

Gilgai is an Australian aboriginal term for water hole, which refers to the water that collects in the depressions formed in these natural wave-like surface patterns. Figure 1 shows a hypothesis about the seven stages of development of a normal gilgai, which are discussed below.

1. Deposition. The clay is laid down in roughly horizontal layers.
2. Drying. Primarily horizontal and vertical shrinkage cracks develop in the upper soil layers in contact with the atmosphere.
3. Major shrinkage cracks. The spacing is largely determined by the type of mineral in the clay. The more active clay minerals will crack more frequently. These cracks become the determining factor in the future development of the gilgai.
4. Heaving around major cracks. Since gilgai are rarely found outside of a climatic region where around 6 to 60 in. (15.2 to 152 cm) of rain fall each year, it is apparent that their development requires an abundant supply of moisture alternating with drying influences. When the soil is cracked and water becomes available again, the water runs to the roots of each crack and the soil there swells upward and causes conical shear failures to occur around each crack. The swelling soil at the roots of the cracks begins to extrude upward within the crack. Mounds that are characteristic of the gilgai form at this stage.
5. Infiltration and leaching. Rainwater and surface runoff are trapped in the depressions between the mounds. Soluble salts are carried with the water as it percolates downward, generally following the cracks opened by shrinkage (stages 2 and 3) and heaving (stage 4). As a result of this leaching, it is not uncommon to find the soil pH tending toward neutral in the depression. There is a possibility that an alteration of the soil type may take place beneath the depressions as fresh water replaces the salt or brackish water that was present when the soil was deposited. The soil beneath the depression is darker than the soil under the mound possibly because of the replacement of saltwater and possibly because of the infiltration of organic materials.
6. Pressure zones and evaporation. The gilgai now begins to take on its mature form as expansion pressure zones begin to form at the root of the shear failure cracks on the boundary between the mound and depression soils. These boundary cracks are formed by the expansion and contraction of the soils in the depressions. Water from the depression feeds in beneath the mounds and evaporates there leaving behind calcium carbonate concretions that are remnants of the salts that have been leached and redeposited. These nodules are generally found only under the mounds. The soils beneath the depressions remain wet throughout the year.
7. Maturity. The mature gilgai profile is shown in Figure 1, stage 7. Its surface features are the mound and the depression. Below the surface, there is the saturated zone beneath the depression, the pressure zone, the intrusion zone at the root of the major genetic cracks, and the evaporation zone where carbonate concretions are found. Seasonal moisture variations cause an increase in the relative elevation of the mound and the depression, both of which rise during wet weather and subside in the dry seasons. There is a greater change of moisture content beneath the mound than in any other location.

Figure 1. Stages of genesis of normal gilgai.

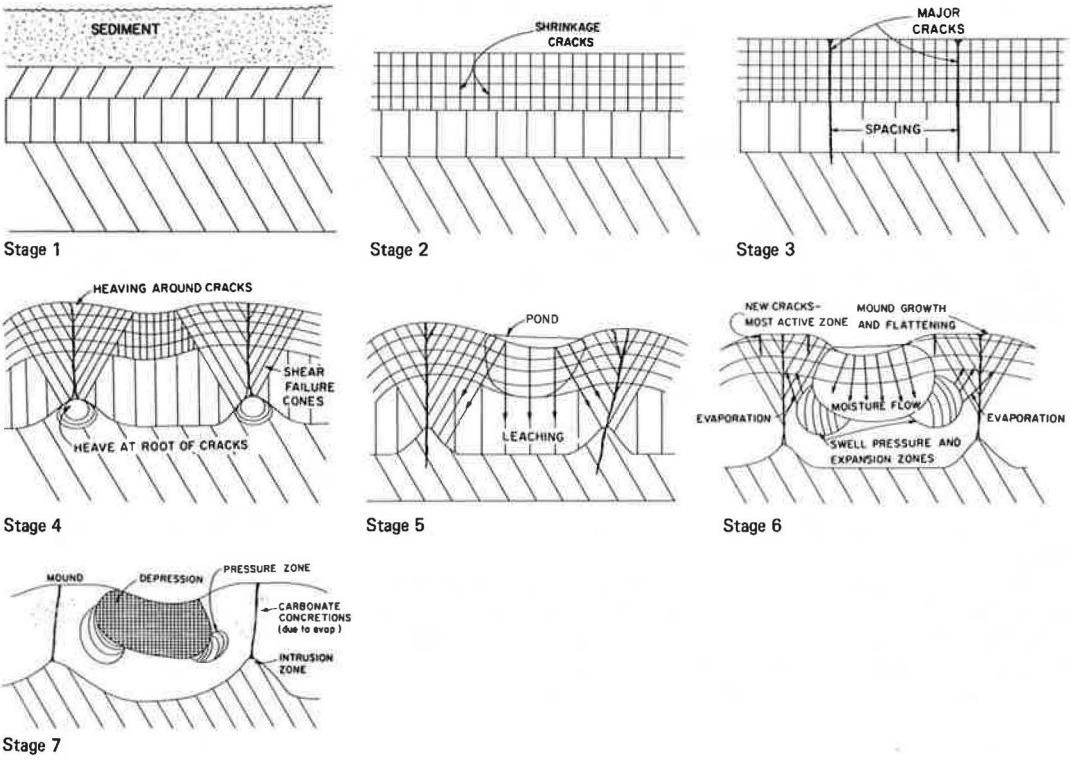

Figure 2. Variations in gilgai soil profile.

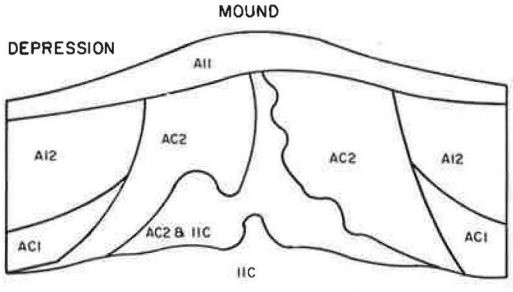

Table 1. Laboratory characterization of gilgai samples.

Horizon	Sand:Silt:Clay (percent)	USDA Texture	pH	Soil Bulk Density (g/cm^3)	At-Field Volumetric Water Content (percent)	Liquid Limit (percent)	Plastic Limit (percent)	Electrical Conductivity (m℧/cm)
A11[a]								0.351
A11D[a]								0.234
A12	11:32:57	Clay	7.3	1.47	44.18	57	27	
AC1	12:36:52	Clay	7.8	1.51	37.46	60	27	0.681
AC2	15:34:51	Clay	7.6	1.52	37.37	52	28	
AC2 and IIC	10:37:53	Clay	7.6	1.59	38.90	67	27	
IIC	5:48:47	Silty clay	7.8	1.69	39.17	62	28	

Note: 1 m℧/cm = 1 mS/cm.

[a]Mount depression.

The most important element in the genesis of a gilgai is the formation of major cracks. The spacing of the cracks depends on the mineralogy, and the cracking patterns that form are responsible for all subsequent behavior of the gilgaied profile. Even though the soil may be reworked to a depth of several feet (meters) during construction, the cracking patterns remain in the natural soil below the reworked zone and, as such, constitute a source for the reestablishment of the roughness patterns. Gilgai fields that have been plowed have been found to reestablish the same patterns in the same locations as before within 2 to 11 years after they were disturbed (1). Figure 2 shows the vertical profile of a gilgai that was observed in a field study site in Snook, Texas. Various soil types were identified within the section primarily by color although their natural water content and pH values were major distinguishing characteristics. Table 1 gives several measured characteristics of each of these soils. There are four major points in Table 1:

1. Bulk density. The bulk density of the A2 soil is lowest of all and is closely followed by the AC1 and the AC2 soils. All of these are in the depression area indicating that they have swelled more than the AC2 and IIC soils. This is in accordance with the field observation that the soils beneath the depression remain wet while the soils beneath the mounds fluctuate in moisture content with the seasons.
2. pH. The pH of the A12 soil is lower than all others and close to neutral (pH = 7.0). This indicates the effect of a long period of leaching that dissolves calcium carbonate salts.
3. Electrical conductivity. The electrical conductivity of the surface soils, A11, is different between the mound and the depression. The higher conductivity over the mound indicates the presence of a higher salt concentration in that soil. This indicates that it may be a zone of accumulation of the dissolved salts and leaching water.
4. Atterberg limits. Although there are some distinctions to be made between the soil types, the Atterberg limits for all the soil types are roughly the same. The sole exception is the AC2 soil that has a lower liquid limit, presumably because of its higher sand content. The point to be observed here is that Atterberg limits could not be used to identify the presence of a gilgaied profile.

Seasonal Movements

Gilgai will usually develop in a field that has low slopes and is poorly drained. This was the case with the field near Snook, Texas. Despite their unusually wet condition, the gilgai still experience shrinking and swelling as water enters and leaves the soil. Spotts (2) instrumented several of these gilgai and measured the vertical strain with depth, horizontal strain at the surface, soil suction (with a tensiometer), and volumetric water content with a nuclear, moisture depth probe. Various other climatic and hygrometric data were recorded and presented in Spotts' dissertation. Measurements were begun when the soil was at its driest during August 1973 and continued on until December of that year by which time the soil had become thoroughly wet. As shown in Figure 3, the major vertical strain was measured beneath the mound. Figure 4a shows the initial suction contours as measured by tensiometer, and Figure 4b shows the final suction contours. The largest change of suction took place beneath the mound. Changes in volumetric water content showed roughly the same patterns. One major finding of this field study was that water moves rapidly through the soil even in such a wet and swollen condition. This is a strong indication that the cracking fabric of the clay plays a major role in transporting moisture within the clay mass. These data call for a careful review of our concepts of field mass permeability.

Characteristic Shapes of Gilgai

As shown in Figure 5, the surface profile of a gilgai in Snook closely resembles that of a sine wave. In fact, regression analysis of the surface elevations against a sine wave

Figure 3. Maximum vertical strain in Snook gilgai.

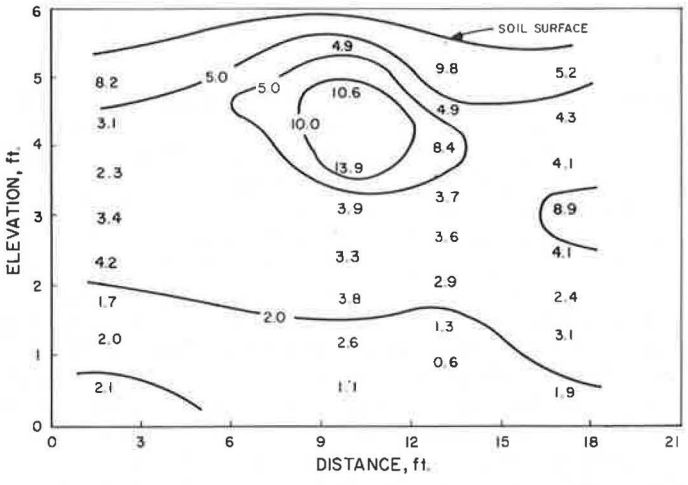

Figure 4. Contours of (a) initial suction and (b) final suction.

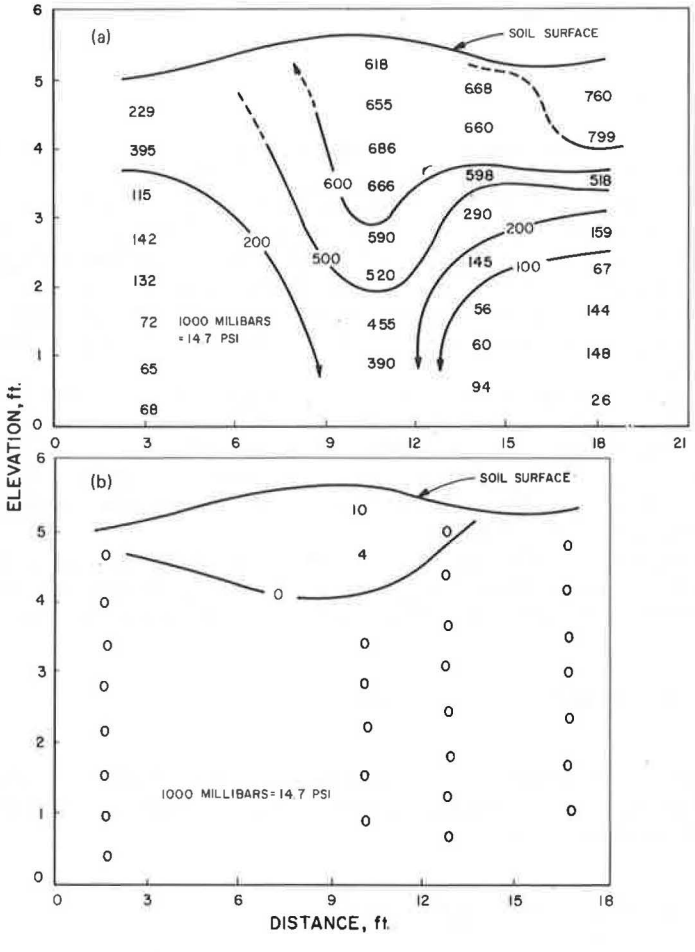

Figure 5. Vertical profile of Snook gilgai.

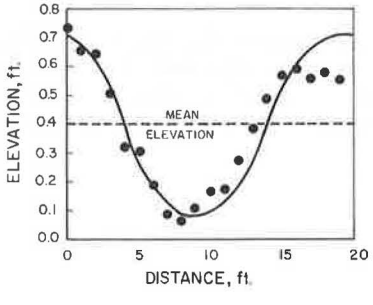

fitted through the data, showed correlation coefficients R^2 between 0.86 and 0.98. Figure 6 is an aerial view of the field at Snook, showing the overall gilgai pattern. The white building in the photograph is the shed housing the instrumentation used by Spotts. Pedologically, the Snook field is in the Burleson clay and the Thrall, Texas, field is in the Houston Black clay. Geologically, the Snook field is in the Brazos River floodplain and is a recent alluvium. The Thrall field is in the Taylor formation. Both fields have about the same mixture of minerals (>40 percent montmorillonite and <10 percent kaolinite); the only distinction between them appears to be in the percentage of clay and the pH. The Snook field has between 40 and 66 percent clay, and the Thrall field has between 55 and 62 percent. The pH is between 7.0 and 8.1 at Snook, and it is between 7.7 and 8.0 at Thrall. There is slightly more calcium carbonate in the Thrall soil. Based on the minor variations of soil properties in these two formations it was expected that the distributions of wavelengths and amplitudes that could be measured in these fields would be very nearly identical. This was shown to be the case. Two kinds of surveys were run to determine these distributions: a field survey and a grid survey for use in a Fourier analysis.

Field Survey

Radial lines were laid out from the leveling instruments set at random in each field. A steel tape was used to measure distances to the tops of the mounds along each radial line. Relative elevations of each of these were recorded. A wavelength was taken as the distance between two successive high points. An amplitude was taken as one-half of the difference between the low point and the average of the high points. A total of 182 points were collected in the Snook field along rays that varied in length from 50 to 650 ft (15.2 to 198 m). A total of 83 points were collected at the site near Thrall. Table 2 gives the statistics of the amplitude and wavelength frequency distributions for Snook and Thrall.

Analysis of variance of the two distributions of wavelengths and amplitudes shows that neither their means nor their standard deviations are significantly different at the 95 percent confidence level. Thus, whatever differences may exist between the Snook and Thrall soils, their effect does not make much practical difference in the gilgai wavelengths or amplitudes. The wavelength frequency distributions are shown in Figures 7a for Snook and 7b for Thrall.

Because of such wide coefficients of variation for both wavelength and amplitude, any simple relation between amplitude and wavelength would be expected to have a low correlation coefficient. This was the case for the Snook gilgai,

$$a = 0.031\,\lambda^{0.58} \quad (R^2 = 0.10) \tag{1}$$

where a = amplitude and λ = wavelength in feet (meters). The Thrall gilgai had a somewhat better correlation coefficient of 0.46, and its equation relating amplitude to wavelength is as follows:

$$a = 0.028\,\lambda^{0.77} \quad (R^2 = 0.46) \tag{2}$$

Despite the fact that there were no statistically significant differences between the amplitude and wavelength distributions, the exponents on each of these two equations differ by 0.19. This is an indication of how widely scattered the data are. The coefficient of variation of the Snook data is around 60 percent, and that of the Thrall data is about 40 percent.

Figure 6. Aerial view of Snook gilgai field.

Table 2. Gilgai wave characteristics.

Item	Snook Gilgai		Thrall Gilgai	
	Wavelength	Amplitude	Wavelength	Amplitude
Mean, ft	19.0	0.200	17.7	0.272
Standard deviation, ft	7.63	0.099	8.37	0.138
Skewness	-0.66	-0.71	-0.56	-0.30
Coefficient of variation, percent	40	50	47	51

Note: 1 ft = 0.3 m.

Figure 7. Wavelength probability density function.

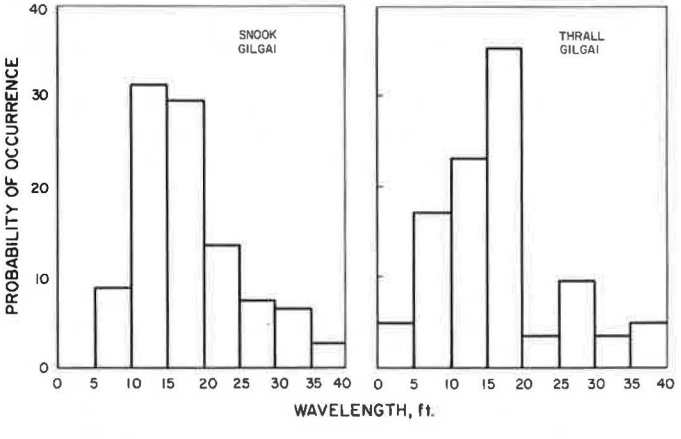

Grid Survey

At Snook, elevations were measured every 5 ft (1.52 m) within a 100 by 100-ft (30.5 by 30.5-m) square grid, and each of the rows and columns of the grid was analyzed separately to determine its characteristic roughness patterns. The vertical profile of each line was assumed to be made up of sums of cosine waves of the following form:

$$u(x) = \sum_{i=1}^{n} a_i \cos \frac{i\pi x}{L} \tag{3}$$

where $u(x)$ is an elevation measured relative to the average elevation of the section. Solution of simultaneous equations resulting from equation 3 gave amplitudes that corresponded with the various specific wavelengths. Regression analysis of the mean amplitudes for each given wavelength resulted in the following equation:

$$a = 0.030\ \lambda^{0.20} \quad (R^2 = 0.32) \tag{4}$$

The exponent on equation 4 is 0.20, which is a factor of 2.9 lower than the exponent, for the same field, based on directly measured data. A certain amount of this discrepancy can be explained by the scatter of the data. The rest of the difference may be sought in the different approaches taken by the field survey and the grid survey. The field survey assumed each gilgai shape to be sinusoidal but not periodic. Thus, each distance peak-to-peak was taken at the single wavelength with a single amplitude. The Fourier analysis of the grid data assumed each shape between peaks to be made up of the sum of several sine waves of varying wavelengths and amplitudes. Thus, what is listed as an amplitude in the field survey is the sum of several amplitudes in the Fourier analysis. Thus, it is reasonable to expect that the exponent relating amplitudes and wavelengths in a Fourier analysis will be smaller than that taken from survey data; in this case, the factor relating the two exponents is 2.9.

Mineralogy-Wavelength Relations

The proof that mineralogy determines the spacing of the cracks and thus the wavelengths of expansive clay roughness consists of two parts. First it must be shown that fields in different geologic formations but with similar mineralogical mixtures have similar amplitude and wavelength distributions. Secondly, it must be shown that fields with different mixtures of minerals have significantly different amplitude and wavelength distributions. The first part of this proof has been verified for the Snook and Thrall fields. Further work on the second part of this proof is presently under way.

EXPANSIVE CLAY ROUGHNESS OF PAVEMENTS

The GM profilometer was used to measure the profile of pavements in the vicinity of the Snook and Thrall fields. One other set of profilometer runs was made on the Old San Antonio Road, a rough pavement that was built on the Burleson clay, about 20 miles (32.2 km) from Snook. This pavement section was chosen because of its similarity in mineralogy to both the Snook and the Thrall fields and because it was desirable to obtain data on low-serviceability-index pavements. There are two ways of analyzing the profilometer data: (a) by a fast Fourier transform (3, 4) of both the right and left wheel paths (5, 6) and (b) by profile filters. The filters were designed according to a pro-

cedure developed by Gimlin, Cavin and Budge (7) for the bands of wavelengths given in Table 3.

The profile data are in digital form, sampled every 2.03 in. (5.15 cm) along each wheel path. The filters are digital filters that are designed to pass only those amplitudes of waves within the wavelength band specified. The filter consists of a set of coefficients, in this case, 172 of them. So that the ordinate of the filtered data at station i can be obtained, the ordinate of the unfiltered data at station i-j is multiplied by the coefficient c_j and added together with 172 other such terms as shown in the following equation:

$$\alpha_i = \sum_{j=1}^{172} c_j a_{i-j} \tag{5}$$

where α_i is the ordinate of the filtered data, and a_{i-j} is the ordinate of the unfiltered data at station i-j.

Figure 8 shows the results of the application of these filters to pavement sections at Snook, Thrall, and the Old San Antonio Road. It is significant that these sections, all on expansive clay subgrades, show higher amplitudes for wavelengths around 13 and 30 ft (3.9 and 9.1 m), the same range of dominant wavelengths that were indicated by the field surveys in Snook and Thrall. Figure 8 also shows the distinctive growth of amplitude as the pavement gets rougher and the serviceability index decreases. A total of 14 pavement sections were measured with serviceability indexes (SI ranging between 1.7 and 4.5). A best fit polynomial that relates SI to wavelength and amplitude was as follows:

$$SI = 5.00 + 0.1774\lambda - a(126.4 - 0.1665\lambda^2) + a^2(1{,}688.4 - 21.99\lambda) \quad (R^2 = 0.92) \tag{6}$$

The standard error on this equation is 0.22 serviceability index units. Amplitudes are in inches (centimeters), and wavelengths are in feet (meters).

A special filter was designed to scan through the profilometer data, find the high points of the bumps, and measure the distance between the high points. This filter copies the effect of a field survey such as conducted in the gilgai fields at Snook and Thrall and was intended to determine whether the frequency distribution of wavelengths on the pavements was the same as those in the adjacent fields. Results of the filter runs at the Old San Antonio Road, Snook, and Thrall are shown in Figure 9. These distributions are similar to those determined by the field survey, indicating that the same expansive clay roughness patterns are developing beneath the pavement. Especially noticeable is the dominance of peak-to-peak distances of around 15 to 30 ft (4.6 to 9.1 m). These distances have emerged in every analysis of pavement or field as most characteristic of these expansive clay deposits.

RIDING QUALITY OVER EXPANSIVE CLAYS

There are various mechanical means of measuring riding quality, but the Mays meter was selected for this study since its measurements have been shown to correlate well with panel ratings of serviceability index (3). Its ruggedness of construction and its ease of use recommend it for rapid surveys of roughness of pavement sections. The response of the Mays meter to excitation from roadway roughness varies with the frequency of the vibration. Computer program DYMOL (9), which has been modified for use on IBM computers, was used to obtain frequency response of the Mays meter. DYMOL solves the equations of motion of a vehicle mass and the four tire-axle masses.

Table 3. Digital filter characteristics.

Filter No.	Frequency Range[a] (cycles/ft)	Wavelength Band[a] (ft/cycle)	Median Wavelength (ft)
A	0.20 to 0.30	3.3 to 5.0	4.15
B	0.219 to 0.164	6.1 to 7.75	6.80
C	0.069 to 0.0808	12.3 to 14.4	13.35
D	0.054 to 0.0645	15.5 to 18.5	17.0
E	0.0441 to 0.0505	19.8 to 22.6	21.2
F	0.0315 to 0.0347	28.8 to 31.6	30.2
G	0.0221 to 0.025	39.6 to 45.2	42.4
H	0.0126 to 0.0157	63.4 to 79.4	71.4

Note: 1 ft = 0.3 m.

[a]For maximum filter response. Each filter will also respond to waves with frequencies slightly outside of its band.

Figure 8. Serviceability index relations for wavelength versus amplitude.

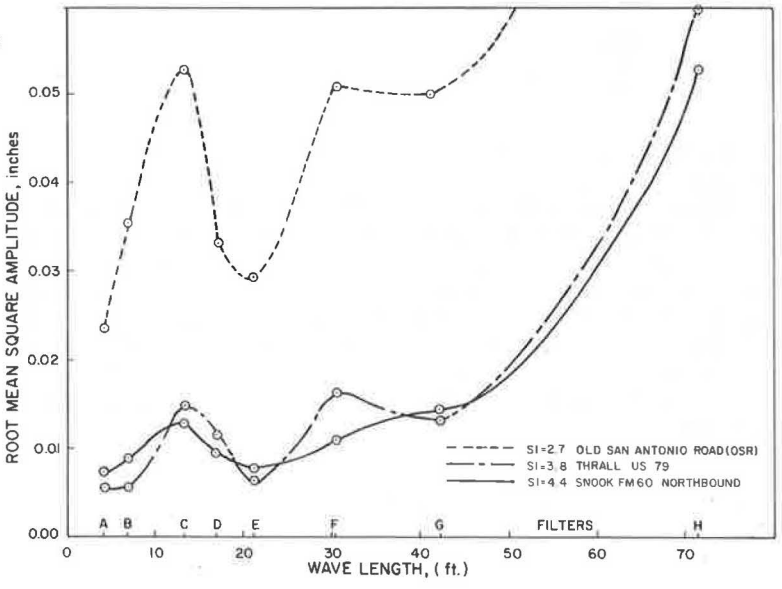

Figure 9. Probability density functions of peak-to-peak distances for left wheel path.

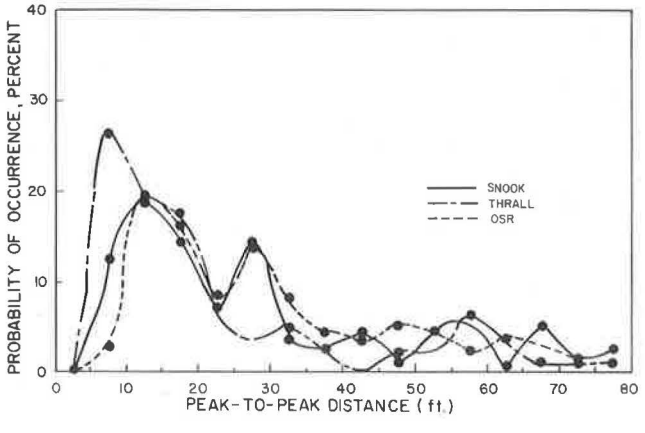

Figure 10. Frequency response curve for computer-simulated vehicle body movement.

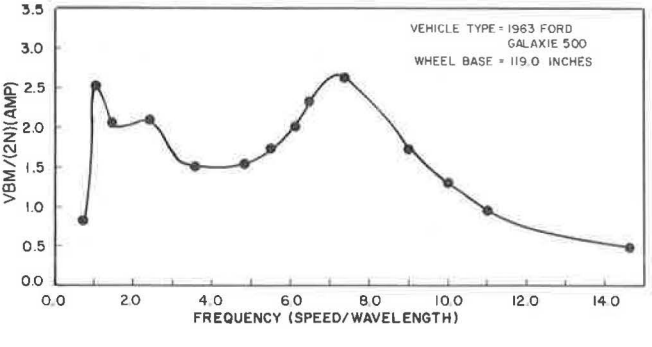

A 1963 Galaxie Ford whose mass and suspension characteristics are published in the literature (10) was the simulated vehicle carrying the Mays meter. The Mays meter accumulates all movements of the rear axle toward and away from the vehicle body. This response of the Mays meter may be compared with the actual up and down movement of the pavement surface, and the resulting Mays meter response curve is shown in Figure 10. These data were developed by simulating runs of the 1963 Galaxie Ford over series of sine waves of varying wavelengths. The Mays meter reading is recorded in inches per mile (centimeters per kilometer), and if the road roughness is considered to be composed of a series of sine waves of varying wavelengths λ_i with a probability of occurrence p_i, then the Mays meter reading for any given section of pavement will be

$$M = b\left[3{,}300 \sum_{i=1}^{n} p_i g_i\left(\frac{v}{\lambda_i}\right) a_i\right]^m \tag{7}$$

where a_i is the amplitude of the wavelength λ_i previously mentioned, v is the speed of the vehicle, and $g_i(v/\lambda_i)$ is the Mays meter response in terms of the frequency of excitation v/λ_i. The constants b and m are needed to account for the effect of the different mass and suspension systems built since 1963. For a typical 1972 Ford, b is 4.0 and m is 0.56. The results of the application of this formula to estimating the riding quality of the section of pavement are shown in Figure 11. Since the Mays meter is normally run at 50 mph (80.5 km/h), the values of serviceability index shown on those curves were determined by the ordinate of each curve at 50 mph (80.5 km/h), using correlations of Mays meter readings with the serviceability index such as the following (1 in./mile = 1.6 cm/km):

Serviceability Index	Mays Meter Reading (in./mile)	Serviceability Index	Mays Meter Reading (in./mile)
4.5	6	2.5	25
4.0	10	2.0	32
3.5	15	1.5	42
3.0	20		

The wavelength distribution chart for the Snook gilgai (Figure 7) was used to establish the probability of occurrence of each wavelength.

DYNAMIC TRAFFIC LOADING DUE TO EXPANSIVE CLAYS

Dynamic load factors were determined by DYMOL simulation of a dump truck running across a simulated pavement with sine-wave roughness. The dump truck had a rear axle load of 17.62 kips (78.3 N) (9), which was for all practical purposes the same as an 18-kip (80-N) single-axle design load. The dynamic load factor was defined as follows:

$$d = \frac{F_{max} - F_s}{F_s} \tag{8}$$

where F_{max} is the maximum dynamic load resulting from the sinusoidal excitation, and F_s is the static load on the tire. If this dynamic load factor is divided by the amplitude

Figure 11. Serviceability index relations for vehicle body movement versus speed.

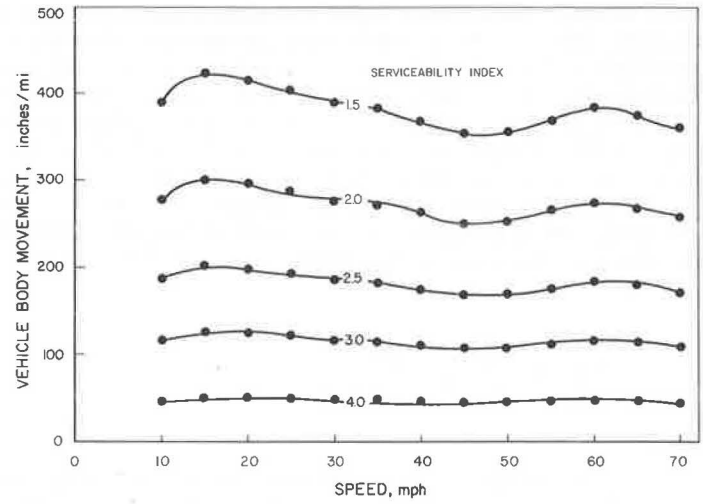

Figure 12. Frequency response curve for vehicle stiffness.

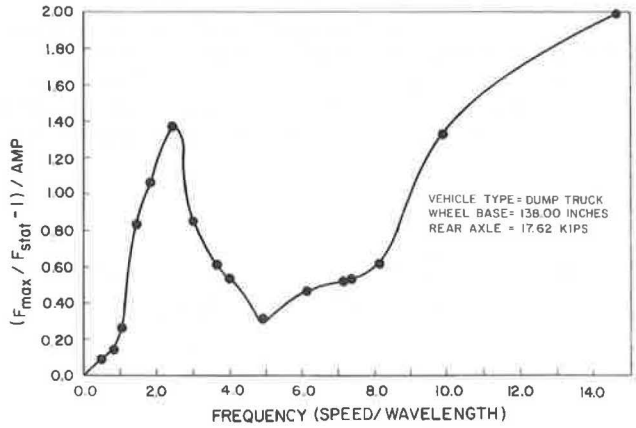

Figure 13. Serviceability index relations for root-mean-square dynamic load factor versus speed.

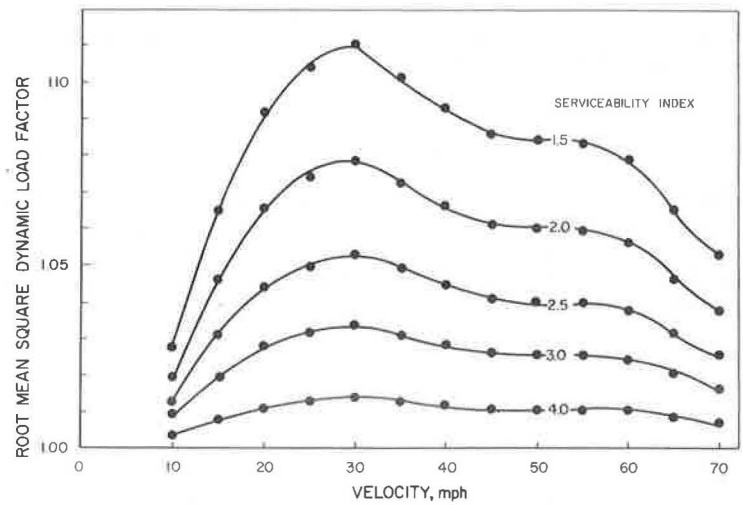

of excitation a to produce a system stiffness number k,

$$k = \frac{d}{a} = \left(\frac{F_{max}}{F_s} - 1\right)/a \tag{9}$$

then it is found that there is a single curve that relates k to the frequency of vibration. This is shown in Figure 12. The shape of the frequency response and the frequencies at maximum response for this dump truck are similar to those calculated by analog computers (11, 12) and measured in field tests (13). The root-mean-square total dynamic load is a measure of the total load applied to the pavement. The equation for the total dynamic load factor including a root-mean-square dynamic component is

$$d_t = 1 + \frac{1}{\sqrt{2}} \sum_{i=1}^{n} p_i k\left(\frac{v}{\lambda_i}\right) a_i \tag{10}$$

where, as before, p_i is the probability of occurrence of the wavelength λ_i, and a_i is the amplitude of that wavelength, which is a function of serviceability index. This equation was used to determine the dynamic load factor versus speed relations shown in Figure 13. The maximum dynamic loads are applied to the pavement surface when the vehicle is traveling at about 20 to 40 mph (32.2 to 64.4 km/h).

The dynamic load factor term was incorporated into the performance equation of the Texas flexible pavement design system to determine by how much the dynamic loads due to expansive clay roughness will shorten pavement service life. It was found that including the dynamic load factor made practically no difference in the service life regardless of the level of roughness. This is not necessarily the case where cracking is concerned; however, the speed of crack propagation varies as the stress intensity factor to the fourth power (14). The stress intensity factor is, in turn, directly proportional to the applied stress. If the applied stress is 1.05 times greater than the static stress, as is the case with an SI of 2.5, then the rate of propagation of a crack due to traffic loading will be 50 percent faster when the pavement is rough than when it has an SI of 4.0. This is a major incentive to maintaining high riding quality on pavements and overlays.

PREDICTION OF REHABILITATION REQUIREMENTS

A reliable prediction of the rehabilitation requirements for a pavement that has been roughened by expansive clay depends on at least three factors: (a) the percentage of the road to be reworked, (b) the amount of releveling to be done by heater-planer or other methods, and (c) the amount of level-up and overlay material to be used. The kinds of calculations that would be required to estimate the amount of material are shown in equation 11 for the simple case for which no releveling is to be done. In this case, the amount of level-up material required to fill the hollow between two successive peaks is the product of the amplitude and the wavelength. Then the existing peaks will be overlaid to depth b above the peaks. The relation between amplitude and wavelength for a serviceability index of 2.5 is taken from equation 6 and substituted into equation 11 below. The serviceability index of 2.5 is chosen here, for it is common practice to overlay at around that level. If p_i is the probability that a given wavelength λ_i will occur, and p_r is the percentage of the roadway that must be reworked, then the total amount of material required for rehabilitation is

$$M = p_r L \sum_{i=1}^{n} p_i a_i \qquad (11)$$

where n is the number of significant amplitudes in the pavement, and L is the project length. Once it is possible to predict when the pavement will need to be reworked in the future, this quantity of material M is multiplied by its unit cost and may be used in estimating the present value of the rehabilitation work. This cost may then be compared with the cost of various kinds of preconstruction treatment such as ponding, wet compaction, chemical treatment, deep-plowed lime or pressure injection at critical points along the pavement such as intersections, grade-crossings, and underpasses. If the cost of pretreatment is higher than the rehabilitation cost, then the designer may normally decide not to use pretreatment. A more usual case may be that a certain amount of pretreatment will greatly reduce the future rehabilitation work to be done or will delay it considerably. In either case, a systems approach to rehabilitation will be able to arrive at the right mixture of preconstruction treatment and rehabilitation.

CONCLUSIONS

1. There is a strong indication that cracking patterns determine roughness patterns.
2. Mineralogical information such as can be provided by pedologic surveys conducted by the Soil Conservation Service and state agricultural universities may give valuable indications of the kind of roughness to expect. One can conclude that the mineralogical mixture of a clay soil may provide valuable information for roughness predictions because there was not a great difference in the mineralogical makeup of the soils at Snook and Thrall and because there were no statistical differences between the means and standard deviations of both amplitude and wavelength distributions in each of the fields.
3. The rate of development of roughness cannot be predicted reliably at present; further study is indicated.
4. Riding quality is greatly affected by expansive clay roughness, but the pavement service life is not altered greatly by the added dynamic load.
5. Digital filters are useful in determining serviceability index relations for amplitude versus wavelength.
6. Field amplitude-wavelength relations are a practical upper limit of the roughness that will develop on a pavement.
7. The development of amplitude-wavelength relations and the prediction of the rate of change of amplitude and the rate of reduction due to preconstruction treatment of the soil will permit planning and estimation of rehabilitation work to be done on a pavement roughened by expansive clay.

REFERENCES

1. G. G. Beckman, G. D. Hubble, and C. H. Thompson. Gilgai Forms, Distribution, and Soil Relationships in Northeastern Australia. Proc., Symposium on Soils and Earth Structures in Arid Climates, Institution of Engineers (Australia), Adelaide, May 1970.
2. J. W. Spotts. The Role of Water in Gilgai Formation. Submitted to the Graduate College, Texas A&M Univ., PhD dissertation, Aug. 1974.
3. R. B. Blackman and J. W. Tukey. The Measurement of Power Spectra. Dover Publications, Inc., New York, 1958.
4. F. D. McCarthy. On the Relation Between Fast Fourier Transforms and Spectral Estimates. Draper Laboratory, Mass., E-2762, May 1973.
5. R. S. Walker and W. R. Hudson. The Use of Spectral Estimates for Pavement

Characterization. Center for Highway Research, Univ. of Texas at Austin, Research Rept. 156-2, Aug. 1973.

6. C. J. Dobbs and J. D. Robson. The Description of Road Surface Roughness. Journal of Sound and Vibration, Vol. 31, No. 2, 1973, pp. 175-183.
7. D. R. Gimlin, R. K. Cavin III, and M. C. Budge, Jr. A Multiple Exchange Algorithm for Calculation of Best Restricted Approximations. Society for Industrial and Applied Mathematics, Journal of Numerical Analysis, Vol. 2, No. 2, April 1974.
8. M. B. Phillips and G. Swift. A Comparison of Four Roughness Measuring Systems. Highway Research Record 291, 1969, pp. 227-235.
9. N. I. Al-Rashid, C. E. Lee, and W. P. Dawkins. A Theoretical and Experimental Study of Dynamic Highway Loading. Center for Highway Research, Univ. of Texas at Austin, Research Rept. 108-1F, May 1972.
10. R. D. Young, T. C. Edwards, R. J. Bridwell, and H. E. Ross, Jr. Documentation of Input for Single Vehicle Accident Computer Program. Texas Transportation Institute, Texas A&M Univ., Research Rept. 140-1, July 1969.
11. A. P. Whittemore, J. R. Wiley, P. C. Schultz, and D. E. Pollock. Dynamic Pavement Loads of Heavy Highway Vehicles. NCHRP Rept. 105, 1970.
12. B. Sinha. Influence of Road Unevenness on Road Holding and Ride Comfort. Institutionen for Maskinelement, Fordonsteknik, Tekniska Hogskolan, Stockholm, Nov. 1972.
13. B. E. Quinn and S. A. Sattaripour. Measurement and Prediction of the Dynamic Tire Forces of a Passenger Vehicle on a Highway. Federal Highway Administration, Rept. FHWA-RD-72-26, Aug. 1972.
14. D. V. Ramsamooj, K. Majidzadeh, and E. M. Kauffmann. The Analysis and Design of the Flexibility of Pavements. Proc., Third International Conference on the Structural Design of Asphalt Pavements, Univ. of Michigan, Vol. 1, pp. 692-704.